IEEE Access
Multidisciplinary | Rapid Review | Open Access Journal

IEEE PHOTONICS SOCIETY SECTION

Received 8 March 2023, accepted 19 April 2023, date of publication 24 April 2023, date of current version 2 May 2023.

Digital Object Identifier 10.1109/ACCESS.2023.3269579

RESEARCH ARTICLE

Interparticle-Coupled Metasurface for Infrared Plasmonic Absorption

ZAKA ULLAH[1,2], ILLANI M. NAWI[3], (Member, IEEE), MUATH AL-HASAN[1], (Senior Member, IEEE), MUHAMMAD JUNAID[4], ISMAIL BEN MABROUK[2], (Senior Member, IEEE), AND ABDUL REHMAN[5]

[1]College of Engineering, Al Ain University, Al Ain, United Arab Emirates
[2]Department of Electrical Engineering, Durham University, DH1 3LE Durham, U.K.
[3]Department of Electrical and Electronic Engineering, Universiti Teknologi Petronas, Perak 32610, Malaysia
[4]Department of Electronic Engineering , Balochistan University of Information Technology, Engineering and Management Sciences (BUITEMS), Quetta, Baluchistan 87300, Pakistan
[5]Department of Information Technology, Balochistan University of Information Technology, Engineering and Management Sciences (BUITEMS), Quetta, Baluchistan 87300, Pakistan

Corresponding author: Muhammad Junaid (m.junaid@buitms.edu.my)

This work was supported in part by Universiti Teknologi Petronas, Malaysia, under Grant YUTP (015LC0-107); and in part by the Abu Dhabi Award for Research Excellence under Grant AARE19-245.

ABSTRACT Plasmonic metasurfaces operating in the long-wavelength infrared region (LWIR) are primarily employed for bio-sensing and imaging applications. The key factor affecting the capability of LWIR metasurfaces is absorption efficiency, whereas significant advances have been made to attain higher absorption intensities, using metal-insulator-metal (MIM) stack structures, which require a complex nanofabrication process and repetition of the patterning process to develop each layer. This study experimentally demonstrates the integration of metasurfaces with plasmonic resonators. The metasurfaces and plasmonic resonators are developed through electron beam lithography (EBL) on the same plane of the Silicon substrate. The fabricated prototype has broad incident angle stability at a bandwidth of 2μm with near-perfect absorption at 8μm resonance wavelength when characterized through the Attenuated Total Reflectance - Fourier Transforms Infrared Spectroscopy (ATR-FTIR) setup. The metasurface device achieves tunable resonance behavior when the incident angles reach up to 70°. The proposed integration of metasurface with plasmonic resonators are well-suited for enhanced biosensing applications with metasurface devices.

INDEX TERMS Absorption, electron beam lithography, metasurface, optical characterization, plasmonic coupling.

I. INTRODUCTION

Plasmonic metasurfaces are 2D surface variants of metamaterials that consist of correspondingly miniaturized resonant metallic structures with sub-wavelength feature sizes [1]. Metasurfaces are ideal tools for plasmonic light manipulation, as they not only direct and concentrate far-field electromagnetic radiation into near-field regions, but also inspire plenty of other exciting applications in the future, including programmable on-demand optics [2] and photonics [3]. In addition, metasurfaces have complete control over light properties such as absorption [4], phase [5], dispersion [6], and polarization [7]. Compared to traditional refractive optics, these recently developed 2D devices have gotten considerable research attention because of their diverse applications, ultra-thin feature, and ease of integration [8]. Various forms of metasurfaces, such as frequency selective metasurfaces [9], high-impedance metasurfaces [10], perfectly absorbing metasurfaces [11], and wavefront shaping metasurfaces [12], are all subject of recent investigations.

The capability of metasurface to perfectly absorb specific optical wavelengths have been commonly utilized and rapidly developed for various applications such as the detection of

The associate editor coordinating the review of this manuscript and approving it for publication was David Caplan.

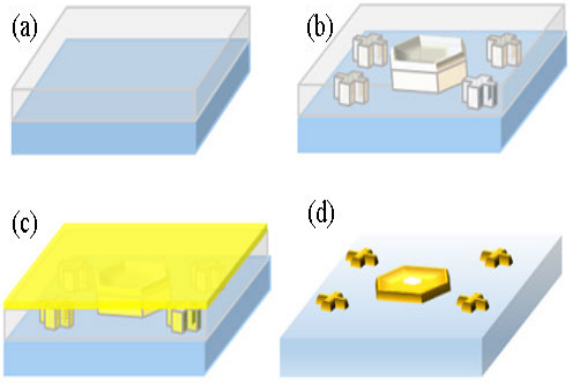

FIGURE 1. The fabrication process of the metasurfaces integrated with a hexagon resonator through EBL. (a) PMMA resist is employed on the silicon wafer with spin coating. (b) Patterning of the proposed structure on PMMA layer with EBL setup and resist development in resist solution. (c) Gold layer deposition on the developed PMMA layers with electron beam deposition. (d) Etching of PMMA layer and unwanted metal through lift-off process to obtain the final prototype.

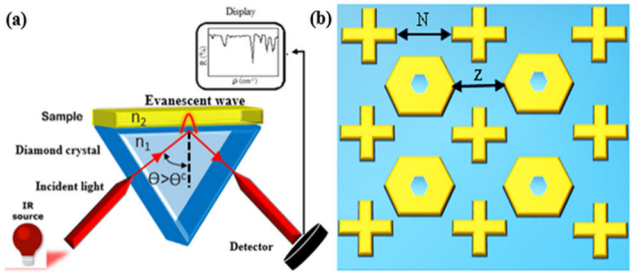

FIGURE 2. (a) ATR-FTIR characterization of the metasurface device: the device is placed on the top of a diamond crystal with close contact, where the effect in absorbance spectra was studied with respect to the change in incidence angle. (b) Illustration of the proposed metasurface device symmetric array for FDTD simulations, N represents the distance between the cross shape metasurface, and Z represents the adjacent space between the hexagon resonators.

near fields [13], [14], bio-sensing, and imaging [9], [15]. Perfect absorption can be attained through the coupling of electromagnetic energy at specific wavelengths by properly designing the absorber structure [16], composition materials, and other attributes of the metasurface absorber structure [17], [18], [19], [20]. Most sensing and imaging systems operate in the long-wavelength infrared region (LWIR) and the Mid-wavelength infrared region (MWIR) ranges. However, their performance is limited due to the narrow-band absorption and the losses of the metallic structures [21]. The broad wavelength absorption in the LWIR range are reported [22], [23], [24] to increase the sensitivity of sensing devices and alleviate the probability of false alarm detection. The problem of low absorption can be modulated by modifying the EM properties of the material, structural optimization, and integration of the metasurface with other photonic devices [25]. Recently, various researchers have developed hybridization techniques [26], [27] by integrating metasurfaces with materials i.e., graphene [15], Vanadium dioxide (VO_2) [28], liquid crystals [29], and Dirac semimetals to achieve high band absorption [30].

Meanwhile, multilayer hybrid structures are being used to alleviate the absorption band limit in LWIR. Most hybrid photonic devices only produce a shift in the operating band and ultimately low absorptivity due to complex structures [31]. In [32], the metasurface is integrated with microelectromechanical systems to enhance the electro-optic performance. Chen et al [33] demonstrated the concept of active VO_2 material in a multilayer metasurface absorber structure at LWIR to achieve high band absorption for sensing purposes. The concept of metasurface vertical stacking is studied in [34], where composite cross-shape absorbers are employed for broadband absorption but sensitive to an incident angle, decreasing the device sensitivity at specific bands. The numerical simulations of hyperbolic metamaterial presented in [35] reveals the broadband absorption by utilizing different-sized tapered hyperbolic metamaterial wave guide in unit cells. The tapered stacked geometry results in near unity absorption along the 1-30 THz range. In other study, the enhanced second-harmonic generation by patterned metamaterials are reported in [36]. The fabricated multilayer pyramid structure being composed of Au/ ZnO stacked layers results in enhanced second-order nonlinear harmonic generation in the visible region. In reference [7], the metamaterial structure is experimentally investigated with a dielectric spacer for effective coupling of surface plasmon modes and thus enhancing the absorption. The techniques mentioned above for higher absorption with multilayered configuration are difficult to fabricate, time-consuming, and associated with high fabrication costs. Using a single layer structure, to realize high-absorption in metasurfaces remains a great challenge for researchers.

Metasurface fabrication is also a challenging problem [37], [38] and depends on the choice of photolithography technology [39], as each process has limits in terms of size and structural quality [32], [40], [41]. In reference [10], a rapid prototyping technique based on a micro plotter is used to fabricate large-area metasurfaces with a printing resolution of 30 mm. Nanoimprint lithography NIL is considered in [34] for the fabrication of corrugated metasurfaces. Although the NIL process has a high throughput and repeatability, it lacks patterning flexibility. In reference [40], metasurfaces are developed by focused ion beam (FIB) lithography, which leads to a weaker plasmonic response and reduced structural quality due to the impinging ions of a focused beam. The core advantage of the EBL over other technologies are the resolution of the critical dimensions, elimination of the diffraction problems in resist, and extremely adaptable technique. Owing to their better structural quality, homogenous thickness, and better performance of the fabricated metasurface prototypes [41], electron beam lithography (EBL) appears as a suitable candidate in nanofabrication.

In this article, a novel approach based on integrating metasurfaces with plasmonic hexagon resonators is proposed and validated, both experimentally and theoretically. The purpose of integrating metasurface is to boost absorption characteristics. The prototype is developed with nanofabrication

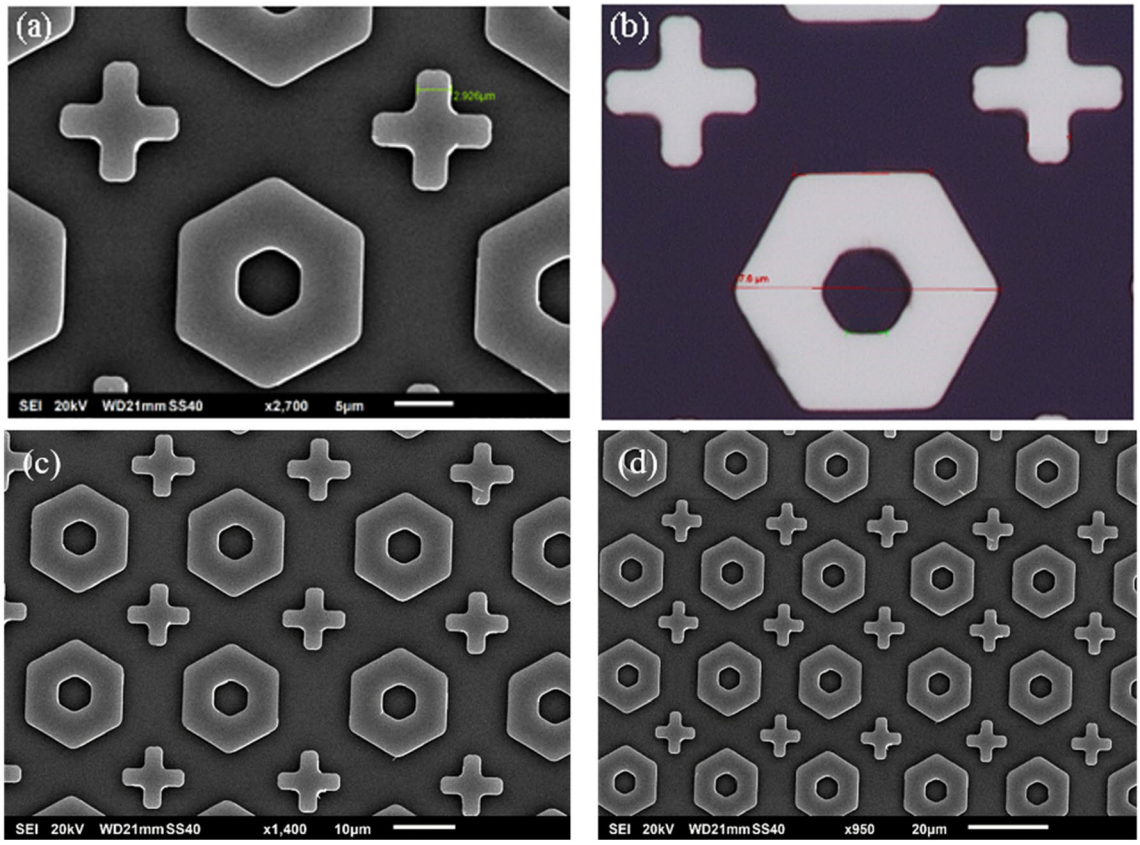

FIGURE 3. FESEM and ATR-FTIR characterization of the metasurface device. (a) FESEM image of the metasurface device obtained with 20KV at 5μm resolution. The image portrays the symmetric pattern of metasurfaces and hexagon resonators with no chemical residue. (b) ImageJ software analysis of the FESEM image, the diameter of hexagon is 17.6 μm and the inner slot radius is 2.6 μm, which are well aligned with our simulation dimensions, The width of the cross metasurface is 2.9 μm and length is 10 μm. (c), (d) Morphology of the fabricated structure with FESEM at 10 μm and 20 μm resolution.

methods by using EBL, resist development, and metal deposition. The symmetric array of the metasurfaces and hexagon resonators are fabricated on the same substrate layer, which eventually reduces the fabrication time and cost compared to multilayered structures. The proposed prototype has a resonance bandwidth of 2μm at the LWIR range with an almost 94% absorption rate when characterized through ATR-FTIR spectroscopy. Furthermore, the stability of absorption resonance is analyzed with different source angles of incidence.

II. MATERIAL AND METHODS

A. DEVICE FABRICATION

The fabrication of cross-shape metasurfaces with integrated plasmonic resonators are developed through electron beam lithography (ELS-7500Ex, ELIONIX INC.) with a silicon wafer as a substrate, as shown in Fig. 1. The gold-coated silicon wafer is cleaned in isopropanol alcohol and dried with nitrogen gas. The EBL positive tone resist, PMMA is spin-coated on a Si wafer at 4000 rpm for 1 minute to obtain a 100 nm thin layer. The thin PMMA layer is prebaked on the hot metal plate at 180 °C for 2 minutes. After the baking process, the wafer is exposed to ELS-7500Ex, to form the desired structure pattern on the PMMA layer. The EBL patterns are created on a 10 mm^2 area with 200 pA electron beam current and a beam dose rate of 450 μC/cm^2, while the acceleration voltage is 50 keV and beamwidth of 20 nm. Subsequently, the wafer with a resist image is developed in a 1:3 MIBK:IPA (Methyl isobutyl ketone: Isopropyl alcohol) solution for 60 seconds. Immediately, the developed PMMA is immersed in distilled (DI) water to stop the developing process and prevent scumming, followed by N_2 blow-drying. The developed patterned PMMA is then post-baked for 90 seconds on the hot plate at 100 °C to remove moisture and residues in the resist.

Subsequently, an electron beam evaporator is used for the metal layer deposition process. A 10 nm chromium and 90 nm gold layer are independently deposited on the developed PMMA wafer at a rate of 1 Å/s. The purpose of the chromium layer is to provide good adherence of the gold layer to the Si substrate. The lift-off process is realized with a 4-hour acetone bath under ultrasonic treatment to remove the PMMA layer and unwanted metal film. Finally, the desired metallic structure on the substrate is washed with DI water. Our proposed metasurface has several advantages over traditional multilayer stacked metasurfaces. Our proposed metasurface design offers advantages over traditional multilayer stacked metasurfaces, including lower fabrication cost and time, due to its single-layer design.

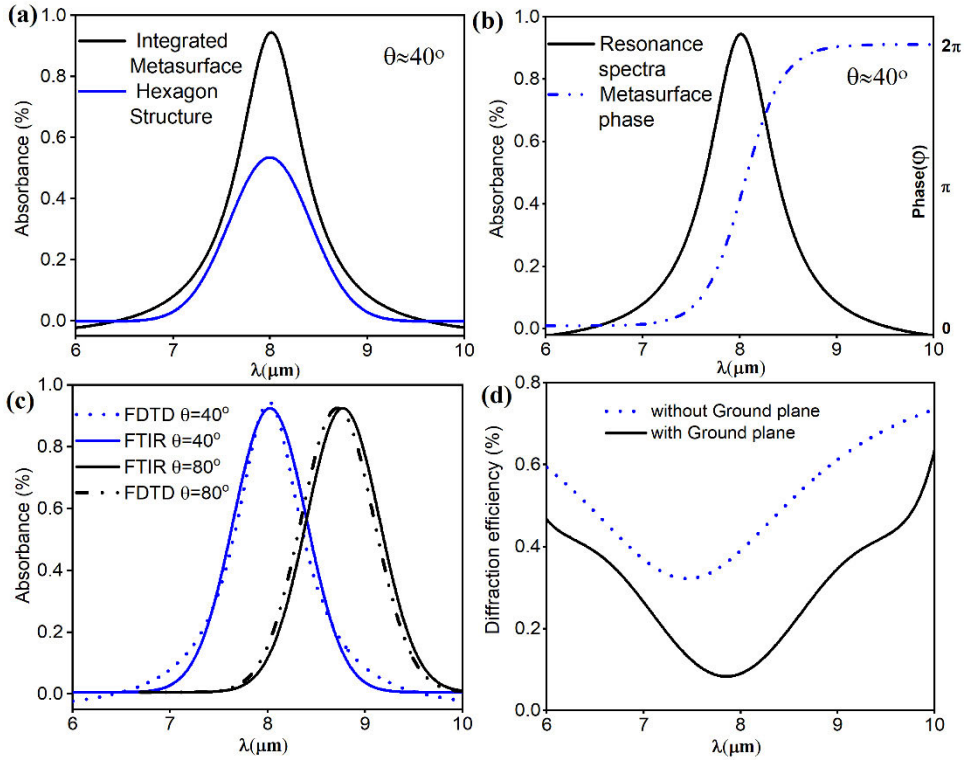

FIGURE 4. Experimental and simulation analysis of the integrated metasurface device, (a) absorption spectra of the hexagon resonator, and integrated metasurfaces. The blue line indicates the absorbance spectra of the hexagon structure obtaining lower absorption at 8um resonance wavelength; when metasurfaces are integrated with hexagon resonator, the absorption and bandwidth improve due to near field coupling between the resonator and cross shape metasurfaces. (b) The simulation spectra of the absorbance indicate the in-phase resonance of the metasurface with hexagon structure. (c) Comparisons of the ATR-FTIR and simulation results, a good agreement is found between the results at 8um resonance wavelength having near-unity absorption. The higher absorption characteristics provide enhanced sensitivity in sensing applications. (d) Diffraction effects on the absorption, the metasurface without ground plane can increase the diffraction, where it can decrease the absorption at the resonant wavelength. However, the ground plane can minimize the diffraction because of the enhancement of plasmonic field at the surface of metasurface.

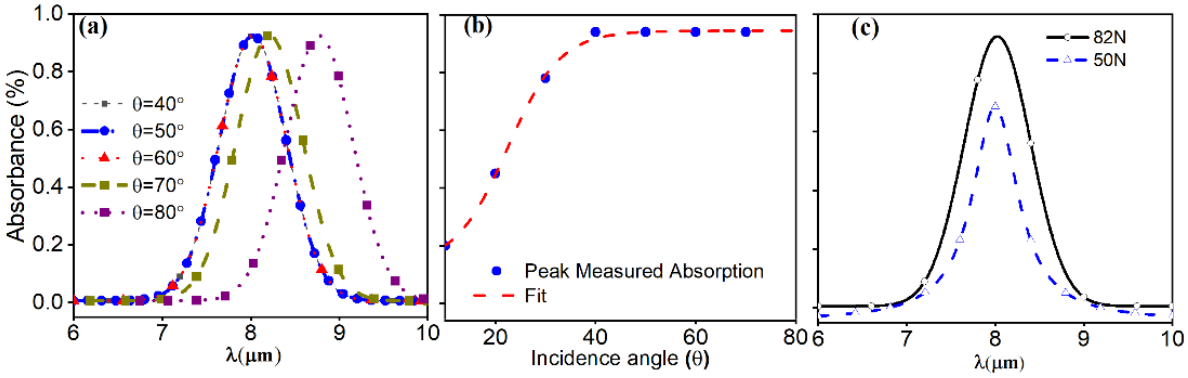

FIGURE 5. The study of the absorption spectra with change in incident angle and ATR force, (a) The absorbance spectra obtained at the near-critical angle of ATR, as the critical angle increased to 60° from 40°, there is no change in the absorption proving the stability of performance at the incident angle range (θ = 40° - 60°). Upon further increasing the incidence angle, the resonance wavelength shifts towards 8.2 μm resonance point. Above the incident angle stable range, the device acquires resonance tunability. (b) The peak value of the absorbance with change in incidence angle, it can be noted when the incidence angle is less than critical angle, the resultant absorption is extremely low. (c) The absorbance spectra were obtained with different ATR forces on the sample to observe the absorbance spectra. At lower force, the sample and crystal have an air gap, which can result in lower absorption because less evanescent field interacts with the sample.

B. EXPERIMENTAL CHARACTERIZATION SETUP

Infrared spectral measurements are carried out using universal attenuated total reflectance coupled with Fourier transform infrared spectrometer (PerkinElmer) ATR-FTIR as illustrated in Fig. 2(a). The fabricated metasurfaces are placed on the diamond crystal facing downward to connect the gold

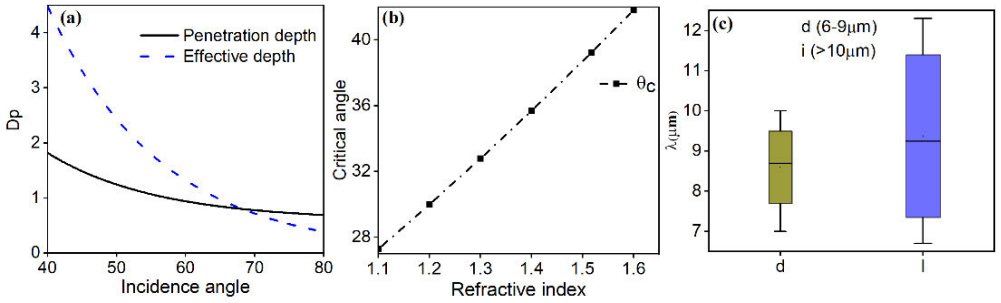

FIGURE 6. Calculation of penetration depth and resonance tuning with change in structural dimensions, (a) The effect of plasmons penetration with change in incidence angle, the penetration depths drop when the angle of incidence reaches to 80^0. (b) The critical angle of ATR is calculated with sample refractive index, lower the refractive index of the sample will require a low critical angle. (c) Adjusting the structural dimensions of the resonator (radius) can change its resonance, leading to a shift in the resonance spectra towards longer wavelengths in the LWIR range.

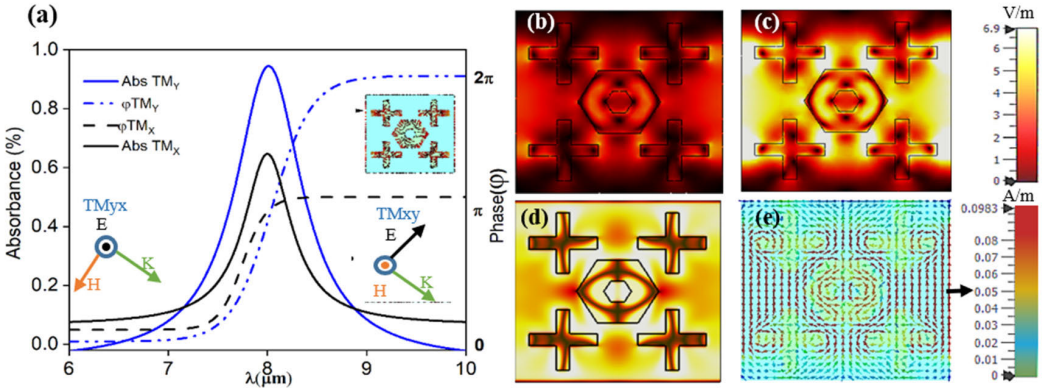

FIGURE 7. (a) Polarization dependent behavior of the metasurface under TMxy and TMyx incidences, The TMyx incidence is the dominant mode of the excite of resonance where the absorption can reach to 94% and significant change in polarization state to $3\pi/2$. (b) Plasmonic field coupling and propagation. The plasmon modes originates on the corners and tips of meta-atoms at TM_{xy} incidence, (c) The effective coupling between the meta-atoms as SPPs travelling towards the center cavity of hexagon under TMyx polarized incidence, (d) The field coupling mode illustrates the field enhancement towards hexagon hotspot, where the mutual coupling between the cross shape metasurface and resonator provide higher absorption due to localized plasmonic fields. (e) The surface currents density to analyze the coupling behavior, as the interaction between the metallic structures provides high density fields.

metasurface layer with the ATR crystal with FTIR resolution of 4 cm^{-1}, gain 1, range 4000 to 650 cm^{-1}, and 20 scans. In this case, the calculated critical angle should be greater than 39^0 so that the evanescent field should penetrate the sample, resulting in surface plasmon resonance. Furthermore, the effect of penetration depth with a change in incidence angle is analyzed to observe the resonance stability and sensitivity by the following formula [43],

$$d_p = \frac{\lambda}{2\pi \left(n_1^2 sin^2\theta - n_2^2\right)^{1/2}} \tag{1}$$

C. FDTD SIMULATION THEORY

Simulations of the proposed metasurface incorporated with plasmonic resonators are carried out using a CST full-wave solver to examine the absorbance spectra. The hexagon geometry is adapted for plasmonic resonators because of structure feasibility and reduced sensitivity with changes in the source angle of incidence. However, the plasmonic resonator has low absorption bandwidth at LWIR. Therefore, cross-shape metasurfaces are employed on the same substrate layer to achieve near-perfect absorption characteristics. The optical properties of Au are adopted from the Palik model [44], [45], whereas the gold thickness (90 nm) is much larger than the skin depth. The skin depth is defined as, $\delta_s = \left(\sqrt{\rho/\pi f \mu}\right)$, where ρ is the resistivity and μ represents permeability. The lower skin depth of gold ($\delta_s = 4.3$-10.7 nm) at LWIR range reduces the direct transmission across the gold structures. The back surface of the S_i substrate is coated with a thin gold layer to minimize transmission and reflectance. The cross shape metasurfaces are equally spaced in array symmetry with N = 17.8 μm distance across the vertical and horizontal axis. The symmetrical distance between the adjacent hexagons resonator is Z = 10 μm, as shown in Fig. 2(b). In simulations, periodic boundary conditions are selected across the x and y directions and perfectly matched layers along the z-direction.

III. RESULTS AND DISCUSSIONS

The surface morphology of the fabricated metasurfaces integrated with plasmonic absorbers is characterized by scanning electron microscopy (SEM) at 20 kV. In Fig. 3(a), the SEM images indicate better EBL print integrity (no residual

layers) and high-fidelity patterns at the micrometer scale over broad areas. The progressive zoom micrograph exhibits the symmetric pattern of metasurfaces and plasmonic absorbers. SEM Images are further analyzed using ImageJ software, to confirm the geometrical measurements of the fabricated design in Fig. 3(b). The high-resolution SEM images portray the uniform continuity of metasurfaces and plasmonic absorbers along the substrate surface. The high-resolution quality of the fabricated prototype can efficiently excite surface plasmon resonance because the metallic structure has fine quality with no defects and deformation in the structural shape. It can be noted, the deformations in the patterning can appear due to the forward and backward scattering of secondary electrons from the writing beam. Where the scattering causes exposure in the unwanted PMMA region. Therefore, in our fabrication dose. In Fig. 3(c), (d) the structural morphology with lower magnifications is presented to show the symmetric metallic array pattern and quality of fabrication with EBL technique.

The integrated metasurfaces with plasmonic resonators are realized with experimental characterization (ATR-FTIR) and theoretically studied through FDTD simulations. The simulation results of the absorption spectra are shown in Fig. 4(a). As it can be depicted, a high absorption is achieved at the LWIR range. The blue line indicates the absorption process, the scattering effect is eliminated with a combination of high accelerating voltage with a low current resonance of a plasmonic resonator (hexagon structure); it is observed that the absorption of the hexagon resonator is significantly lower at 8μm resonance wavelength with almost 50% absorption rate.

Therefore, to achieve high band unity absorption, metasurfaces are integrated on the same plane to couple near-field interaction and suppress far-field radiation loss, thereby improving the resonance bandwidth with higher absorption. The black line in Fig. 4(a) indicates the plasmonic response of hexagon resonator with integrated metasurfaces. The 3dB bandwidth of the integrated structure is 1μm with a peak absorption intensity of 94% at 8 μm. The higher performance is attributed to the cross-shape metasurface enhanced local fields, which is critical for higher absorption efficiency. It can be noted, to achieve a higher resonance response, the phase of the metasurface must be in the resonance range of the hexagon structure illustrated in Fig. 4(b). The in-phase characteristic of the metasurface improves the resonance coupling of the two different structures at the same resonance wavelength. The spacing between the metasurfaces and hexagon resonators allows strong coupling between the adjacent resonators. High absorption can be achieved by tuning the dimensions to overlap resonance and cancel the effect of backscattered radiations spectrally

The experimental results of the absorption spectra through ATR-FTIR are shown in Fig. 4(c). The acquired data of FTIR are corrected with peak fitting to obtain a precise curve of the resonance wavelength. In Fig. 4(c), the blue curve corresponds to the FTIR measurement and is in strong agreement with the FDTD simulation curve with slight discrepancies in absorption peak and resonance bandwidth. These discrepancies can be attributed to the imperfections in the electron beam patterning, whereas in FDTD simulation, ideal geometry is considered. The series of fabrication steps can also affect the absorption spectra of FTIR. The beam resists, chemical etchants, and various cleaning reagents employed in the fabrication process can interfere with surface plasmon resonance of the FTIR spectra because these compounds comprise different bond energies; such factors are again not accounted for in simulations. The close agreement between the FTIR and simulation results at 8μm resonance bandwidth validates the effective near-field coupling of metasurfaces with hexagon resonators resulting in enhanced localized near-field absorption. The literature comparisons with our proposed work are given in Table. 1.

In Fig. 4(d), the diffraction effect on the intensity of absorption is analyzed because the periodicity of the metasurface is regular on the distances when compared to the incident wavelength. Also, the edges, corners, and metal tips are smaller than the wavelength which raises the diffraction effect [46]. During the course of diffraction, some of the energy is absorbed and the rest bounces back on the surface causing secondary plasmon resonance, therefore the diffraction can ultimately reduce the absorption [47]. To reduce the diffraction on the proposed metasurface, we simulated the structure with and without a gold ground plane. The black curve in Fig. 4(d) shows the diffraction efficiency with a gold ground plane. The ground plane will strengthen the evanescent wave by activating surface plasmon resonance. The metallic arrays on the top surface function as couplers, which couples the enhanced evanescent waves into propagating surface plasmon modes, resulting in high absorption. Furthermore, the ground plane acts as reflector which traps the incident energy along with secondary plasmons inside the metasurface. Where the localized field intensities between the hexagon and cross- shape results in higher absorption.

It can be noted, that still diffraction can take some of the energy due to out-of-phase coupling. In our case, the absorption intensity is 94% at resonance wavelength, where 6% energy is taken by the diffraction. The change in resonance position with the ground plane can be attributed is due to the fact that it acts as a shield that blocks the transmission of coupled waves and reduces the losses caused by the environment. Additionally, it helps to match the impedance of the source wavelength to the device resonance wavelength, allowing for maximum energy transfer and improving the absorption performance of the device. The dotted blue curve in Fig. 4(d) illustrates the diffraction behavior without a ground plane. The low intensity of surface plasmon resonance resulting from evanescent waves increases diffraction effectiveness and decreases absorption. The diffraction efficiency increase can be attributed to high transmission and the scattered modes resulting from the diffraction effect on the surface of the metasurface [48].

A. EFFECT OF ATR INCIDENCE ANGLE ON THE ABSORPTION RATE

The stability of the absorption resonance at a broad incidence angle is a key factor for bio-sensing at the LWIR range.

A minimal change or shift in the absorption resonance decreases the sensing efficiency and results in a false alarm; therefore, in this section, the effect of changing the incidence angle on the absorption rate is investigated. Using the ATR setup with FTIR, the first step is to determine the critical angle of ATR with respect to the fabricated device. In this case, a diamond crystal having $n_1 = 2.4$ and the calculated refractive index of the device being $n_2 = 1.518$ are used to estimate the ATR critical angle. These parameters can define the critical angle at which the evanescent waves from the ATR crystal result in the plasmonic resonance. When the incident source has an angle of incidence below the critical angle of ATR, the resultant absorption at the resonance wavelength is minimal. In Fig. 5(a), the absorption spectra with a change in incidence angle are illustrated. The proposed device shows broad-angle stability ranging from ($\theta = 40°$ - $60°$) at 8 μm resonance wavelength with almost unity absorption. Further increasing the incidence angle to $\theta = 70°$, the resonance peak blue shifts towards 8.2 μm resonance wavelength with a drop in absorption at the 8 μm resonance point. It can be nored, that our metasurface shows stability in a certain range of angles, but the resonance shifts at higher angles. This is due to the fact that at higher angles, the incident angle of the electromagnetic wave changes, which affects the effective refractive index of the metasurface. This change in refractive index can cause the resonance to shift.

Consequently, the absorption drastically drops to 10% at 8 μm when the ATR incidence angle is tuned to 80°. However, at $\theta = 80°$, the resonance of the device is further tuned to a 9 μm resonance point. The change in resonance wavelength shows the tunable behavior of the metasurface device. To obtain higher sensitivity in biosensing applications at 8 μm range, the incidence angle should be in the range of ($\theta = 40°$ - $60°$). The effect of peak absorption on the broad incidence angle is depicted in Fig. 5(b), and the blue dots represent the absorption value at a different angle of incidence. An angle less than the critical angle of ATR results in lower absorption. Above the critical angle, the absorption remains stable at unity, but resonance wavelength changes when the incidence angle is tuned from ($\theta = 70°$ - $80°$).

The effect of ATR force on metasurface devices is experimentally studied to observe the absorption spectra. In our case, the sample is solid, which requires force to bring the device surface in close contact with the ATR crystal to achieve adequate absorption intensity. The force must be sufficient so that it may not induce structural defects in the metasurface device, which can result in different resonant wavelength bands. As less force can result in an air gap at the contact interface between the metasurface sample and the ATR crystal. The air gap can also cause a change in the refractive index of the sample. Therefore, the penetration depth of evanescent waves decreases due to the longer path distance leading to lower absorption. The absorbance spectra obtained through ATR depend on various factors, i.e., the area of the device sample contact with ATR crystal and the distribution of a sample within the evanescent field. Figure. 5(c) represents the absorption spectra with different forces applied on the sample through ATR. The black line in Fig. 5(c) illustrates the absorption spectra when a force of 82N is applied to the sample achieving near-perfect absorption at 8 μm. The higher absorption intensity is realized due to the reduced air gap between the sample and ATR crystal with higher evanescent fields interacting with the sample. It can also be noted, that the observed absorbance depends not simply on the area of material in contact with the crystal surface but also on the distribution of the sample within the evanescent field. The intensities increase as air gaps between the sample and the crystal are reduced, bringing more of the sample into the evanescent field. However, the absorption intensity drops to 70 % when the applied force on the sample is adjusted to 50N, as shown in Fig. 5(c). The lower intensity and less operating bandwidth of the absorption spectra at resonance wavelength result from the higher air gap between the sample and crystal surface.

B. IMPACT OF INCIDENCE ANGLE ON PENETRATION DEPTH AND RESONANCE TUNING

In this section, the impact of incidence angle on the penetration of depth of ATR evanescent waves in the metasurface device is studied to observe the resonance tuning and changes occurring in the absorption peak. It can be observed that, when the incident source has an incidence angle near the critical angle of ATR, the evanescent waves have a greater depth of penetration into the metasurface sample of 1.9 μm, as shown in Fig. 6(a). The peak absorption is realized through the effective coupling of plasmons interaction between the cross shape metasurfaces and hexagon resonator. The increase in incidence angle causes an abrupt change in the field penetration depth. In the stable incidence angle range (40° – 60°), the penetration depth drops to $d_p = 1.2$ μm at $\lambda = 8$ μm, although the absorption value remains the same due to the effective coupling of the metasurface and resonators. Upon further increasing the incidence angle beyond 60°, the penetration depth remains constant, resulting in less absorption at the resonance point $\lambda = 8$ μm, but resonant absorption shifts to different resonance wavelengths.

The refractive index of the device plays an important role in determining the critical angle of the ATR crystal. The lower refractive index of the sample yields a significantly less critical angle which, in turns, increases the incidence angle tuning range. In Fig. 6(b), the critical angle is calculated using different refractive indices, providing insight into resonance tuning with a broad incidence angle range. Furthermore, the resonance shifting with tuning hexagon dimension is systematically analyzed in Fig. 6(c). When the hexagon radius is set to a higher value of 9 μm, the absorption resonance shifts towards longer wavelengths (λ = 8-10 μm) and vice versa. The yellow box represents the resonance tuning range with a change in the radius of a hexagon from 6-9 μm. In contrast, the blue box indicates the wavelength tuning range upon further increasing the structure dimensions and greater hexagon slot diameter. The higher resonance tuning range corresponds to the strong near-field coupling of the

TABLE 1. Literature comparison of the results with proposed work.

Refs	Structure/ Material	Bandwidth	Tuning range	Absorption
[49]	Nano-pillars metasurface	0.4 μm	2.2 – 3.6 μm	90 %
[50]	Cross shape Si_3N_4/Gold stake metasurface	0.2 μm	7 - 9	70 %
[51]	Nano disk metasurface with alternating SiO_2 and TiO_2 stacked geometry with GST phase change material	0.022 μm	1.902 – 1.942 μm	-
[52]	Polystyrene thin film metasurface	0.502 μm	9.5 – 11 μm	96 %
[53]	Circular Dichroism metasurface	0.6 nm	0.726 – 0.745 μm	92 %
[54]	Tri layer MIM stacked chiral Metasurface	-	5 – 5.9 μm	63 %
This work	Single layer cross shape metasurface integrated with hexagon resonators	2 μm	7 – 9.5 μm	94 %

sharp outer edges and sharp inner corners of the hexagon in close proximity.

C. POLARIZATION DEPENDENT BEHAVIOUR AND NEAR-FIELD COUPLING

Numerical simulations were performed using CST Studio to reveal the underlying physical process for the EM response of the integrated metasurface under S-polarized (TM_{xy}) and p-polarized (TM_{yx}) incidences. It can be noted, that here a fixed angle of incidence (i.e., $\theta = 40°$) is considered for TM_{yx} and TM_{xy} incidences. From Fig. 7(a), it can be observed that under TM_{xy} polarization incidence, the conversion of the polarization state is limited to π while achieving low absorption intensity. The shift in polarization state occurs from right-handed polarization towards lift-handed polarization. However, the case is different when the metasurface is incidence with TM_{yx} waves. In Fig. 7(a), it can be clearly seen that TM_{yx} is the dominant mode for the excitation surface plasmon resonance. Also, from the phase plot for TM_{yx}, the polarization state in the resonant bandwidth can shift to a double negative (DNG) state. In this state, the permittivity and permeability of the metasurface become negative, where it can realize the high intensity of absorption at the resonant wavelength. Furthermore, the intensity of surface plots related to both incidences validates the absorption intensity, as for TM_{yx} the current density is maximum around all the edges of the hexagon resonator. Although low surface currents intensity can be seen when the incidence is changed to TM_{xy}.

In addition, field enhancement due to the coupling of the metasurface with the resonator is studied to provide insight into the mechanism of absorption. When the incident waves strike the metasurface structure, the plasmonic resonance is excited on the corner and metallic tips. The excitation of plasmon resonance give rise to propagating plasmonic fields. The interaction between the near fields causes the collective coupling resulting in enhanced absorption. From Fig. 7(b) it can be observed that the coupling of cross resonators near-field to the hexagon resonator increases the field intensity on the hexagon surface, where it is effectively absorbed by the microcavity at the center of hexagon geometry. The micro slot work as a plasmon trapping cavity where the coupled field are highly confined, illustrated in Fig. 7(c). In addition, the four V-shapes from the cross-structure work as directing elements that directs the fields towards the hexagon from all side which also increases the field intensity resulting in high absorption, which can be seen in Fig. 7(d). In Fig. 7(e) the illustration of surface currents on the geometry validates the interaction of the field between the resonator and cross shape metasurface, where the intensity of the field is maximum in the center from the mutual coupling.

IV. CONCLUSION

In conclusion, the integration of cross-shape metasurfaces with plasmonic resonators is experimentally demonstrated for the absorption enhancement, required for sensing applications. The metasurface device has absorption resonance at 8 μm wavelength, and the higher absorption intensity is based on the effective coupling of surface plasmons between the metasurfaces and resonators. The EBL technique is used to fabricate high-quality metasurfaces and resonators on the same substrate plane. The integration method reduces the high cost and long fabrication time required in multi-layer stack metasurface fabrication. Furthermore, the effect of relevant parameters on absorption resonance, such as incidence angle, refractive index, and penetration depth, is experimentally analyzed to achieve optimal performance at the LWIR range. The fabricated design can be employed in sensing applications that require spectrally tunable and performance-stable metasurface devices.

ACKNOWLEDGMENT

The authors would like to thank the College of Engineering, Al Ain University, for their support.

REFERENCES

[1] L. Zhang, J. Ding, H. Zheng, S. An, H. Lin, B. Zheng, Q. Du, G. Yin, J. Michon, Y. Zhang, Z. Fang, M. Y. Shalaginov, L. Deng, T. Gu, H. Zhang, and J. Hu, "Ultra-thin high-efficiency mid-infrared transmissive Huygens meta-optics," *Nature Commun.*, vol. 9, no. 1, pp. 1–9, Apr. 2018.

[2] Q. Qian, P. Liu, L. Fan, L. Zhao, and C. Wang, "None sharp corner localized surface plasmons resonance based ultrathin metasurface single layer quarter wave plate," *Sci. Rep.*, vol. 11, no. 1, p. 8956, Apr. 2021.

[3] H.-L. Wang, E.-M. You, R. Panneerselvam, S.-Y. Ding, and Z.-Q. Tian, "Advances of surface-enhanced Raman and IR spectroscopies: From nano/microstructures to macro-optical design," *Light: Sci. Appl.*, vol. 10, no. 1, p. 161, Aug. 2021.

[4] W. Wang, F. Yan, S. Tan, H. Li, X. Du, L. Zhang, Z. Bai, D. Cheng, H. Zhou, and Y. Hou, "Enhancing sensing capacity of terahertz metamaterial absorbers with a surface-relief design," *Photon. Res.*, vol. 8, no. 4, p. 519, 2020.

[5] W. Dong, Y. Qiu, X. Zhou, A. Banas, K. Banas, M. B. Breese, T. Cao, and R. E. Simpson, "Tunable mid-infrared phase-change metasurface," *Adv. Opt. Mater.*, vol. 6, no. 14, 2018, Art. no. 1701346.
[6] V.-C. Su, C. H. Chu, G. Sun, and D. P. Tsai, "Advances in optical metasurfaces: Fabrication and applications [Invited]," *Opt. Exp.*, vol. 26, no. 10, p. 13148, 2018.
[7] V. Nagal, T. Li, J. B. Khurgin, and D. H. Gracias, "Large-area arrays of quasi-3D Au nanostructures for polarization-selective mid-infrared metasurfaces," *ACS Appl. Nano Mater.*, vol. 3, no. 7, pp. 7029–7039, Jul. 2020.
[8] A. Leitis, M. L. Tseng, A. John-Herpin, Y. S. Kivshar, and H. Altug, "Wafer-scale functional metasurfaces for mid-infrared photonics and biosensing," *Adv. Mater.*, vol. 33, no. 43, Oct. 2021, Art. no. 2102232.
[9] A. Nemati, Q. Wang, M. H. Hong, and J. H. Teng, "Tunable and reconfigurable metasurfaces and metadevices," *Opto-Electron. Adv.*, vol. 1, no. 5, 2018, Art. no. 180009.
[10] A. Salmon, M. Lavancier, C. Brulon, L. Coudrat, B. Fix, G. Ducournau, R. Peretti, and P. Bouchon, "Rapid prototyping of flexible terahertz metasurfaces using a microplotter," *Opt. Exp.*, vol. 29, no. 6, p. 8617, 2021.
[11] Y. Chen and J.-S. Li, "Switchable dual-band and ultra-wideband terahertz wave absorber," *Opt. Mater. Exp.*, vol. 11, no. 7, p. 2197, 2021.
[12] J. Xu, D. Jia, Y. Liu, Y. Tian, and X. Yu, "Tunable terahertz metamaterial absorber actuated by thermomechanical bimaterial microcantilevers," *Opt. Exp.*, vol. 28, no. 7, p. 10329, 2020.
[13] M. Hesari-Shermeh, B. Abbasi-Arand, and M. Yazdi, "Analysis of substrated periodic metasurfaces under normal incidence," *Opt. Exp.*, vol. 29, no. 2, p. 1694, 2021.
[14] J. Han and R. Chen, "Tunable broadband terahertz absorber based on a single-layer graphene metasurface," *Opt. Exp.*, vol. 28, no. 20, p. 30289, 2020.
[15] Z. Zhang, X. Qi, J. Zhang, C. Guo, and Z. Zhu, "Graphene-enabled electrically tunability of metalens in the terahertz range," *Opt. Exp.*, vol. 28, no. 19, p. 28101, 2020.
[16] F. Ding, Y. Cui, X. Ge, Y. Jin, and S. He, "Ultra-broadband microwave metamaterial absorber," *Appl. Phys. Lett.*, vol. 100, no. 10, Mar. 2012, Art. no. 103506.
[17] X. M. Wen, Y. G. Bi, F. S. Yi, X. L. Zhang, Y. F. Liu, W. Q. Wang, J. Feng, and H. B. Sun, "Tunable surface plasmon-polariton resonance in organic light-emitting devices based on corrugated alloy electrodes," *Opto-Electron. Adv.*, vol. 4, no. 8, 2021, Art. no. 200024.
[18] K. Yang, W. Yu, G. Huang, J. Zhou, X. Yang, and W. Fu, "Highly sensitive detection of Staphylococcus aureus by a THz metamaterial biosensor based on gold nanoparticles and rolling circle amplification," *RSC Adv.*, vol. 10, no. 45, pp. 26824–26833, 2020.
[19] F. Dong and W. Chu, "Multichannel-independent information encoding with optical metasurfaces," *Adv. Mater.*, vol. 31, no. 45, 2019, Art. no. 1804921.
[20] D. Rodrigo, A. Tittl, N. Ait-Bouziad, A. John-Herpin, O. Limaj, C. Kelly, D. Yoo, N. J. Wittenberg, S.-H. Oh, H. A. Lashuel, and H. Altug, "Resolving molecule-specific information in dynamic lipid membrane processes with multi-resonant infrared metasurfaces," *Nature Commun.*, vol. 9, no. 1, p. 2160, Jun. 2018.
[21] D. Katrodiya, C. Jani, V. Sorathiya, and S. K. Patel, "Metasurface based broadband solar absorber," *Opt. Mater.*, vol. 89, pp. 34–41, Mar. 2019.
[22] Y. G. Jeong, Y. M. Bahk, and D. S. Kim, "Dynamic terahertz plasmonics enabled by phase-change materials," *Adv. Opt. Mater.*, vol. 8, no. 3, 2020, Art. no. 1900548.
[23] J. De Teresa, P. Orus, R. Córdoba, and P. Philipp, "Comparison between focused electron/ion beam-induced deposition at room temperature and under cryogenic conditions," *Micromachines*, vol. 10, no. 12, p. 799, Nov. 2019.
[24] Y. Huang, X. Zhang, E. Ringe, M. Hou, L. Ma, and Z. Zhang, "Tunable lattice coupling of multipole plasmon modes and near-field enhancement in closely spaced gold nanorod arrays," *Sci. Rep.*, vol. 6, no. 1, pp. 1–10, Mar. 2016.
[25] D. Kim, H. Chung, J. Yu, I. Hwang, S. Park, F. Demmerle, G. Boehm, M. C. Amann, M. A. Belkin, J. Y. Jung, and J. Lee, "Spin-controlled nonlinear harmonic generations from plasmonic metasurfaces coupled to intersubband transitions," *Adv. Opt. Mater.*, vol. 8, no. 8, 2020, Art. no. 2000004.
[26] A. K. Azad, W. J. M. Kort-Kamp, M. Sykora, N. R. Weisse-Bernstein, T. S. Luk, A. J. Taylor, D. A. R. Dalvit, and H.-T. Chen, "Metasurface broadband solar absorber," *Sci. Rep.*, vol. 6, no. 1, p. 20347, Feb. 2016.
[27] N. Mou, S. Sun, H. Dong, S. Dong, Q. He, L. Zhou, and L. Zhang, "Hybridization-induced broadband terahertz wave absorption with graphene metasurfaces," *Opt. Exp.*, vol. 26, no. 9, p. 11728, 2018.
[28] V. R. Shrestha, B. Craig, J. Meng, J. Bullock, A. Javey, and K. B. Crozier, "Mid—To long-wave infrared computational spectroscopy with a graphene metasurface modulator," *Sci. Rep.*, vol. 10, no. 1, pp. 1–9, Mar. 2020.
[29] G. Deng, H. Hu, H. Mo, J. Xu, Z. Yin, H. Lu, M. Hu, J. Li, and J. Yang, "Tunable terahertz metamaterial wideband absorber with liquid crystal," *Opt. Mater. Exp.*, vol. 11, no. 12, p. 4026, 2021.
[30] T. Taliercio and P. Biagioni, "Semiconductor infrared plasmonics," *Nanophotonics*, vol. 8, no. 6, pp. 949–990, Jun. 2019.
[31] S. Kumar, "Titanium nitride as a plasmonic material for excitation of Tamm plasmon states in visible and near-infrared region," *Photon. Nanostruct.-Fundam. Appl.*, vol. 46, Sep. 2021, Art. no. 100956.
[32] N. Li, Z. Xu, Y. Dong, T. Hu, Q. Zhong, Y. H. Fu, S. Zhu, and N. Singh, "Large-area metasurface on CMOS-compatible fabrication platform: Driving flat optics from lab to fab," *Nanophotonics*, vol. 9, no. 10, pp. 3071–3087, Aug. 2020.
[33] Z. Chen, F. Qu, Y. Wang, and P. Nie, "Terahertz dual-band metamaterial absorber for trace indole-3-acetic acid and tricyclazole molecular detection based on spectral response analysis," *Spectrochimica Acta A, Mol. Biomolecular Spectrosc.*, vol. 263, Dec. 2021, Art. no. 120222.
[34] R. Sarma, D. de Ceglia, N. Nookala, M. A. Vincenti, S. Campione, O. Wolf, M. Scalora, M. B. Sinclair, M. A. Belkin, and I. Brener, "Broadband and efficient second-harmonic generation from a hybrid dielectric metasurface/semiconductor quantum-well structure," *ACS Photon.*, vol. 6, no. 6, pp. 1458–1465, Jun. 2019.
[35] M. W. Arrays, X. Yin, L. Chen, X. Li, and S. Member, "Ultra-broadband super light absorber based on multi-sized tapered hyperbolic metamaterial waveguide arrays," *J. Lightw. Technol.*, vol. 33, no. 17, pp. 3704–3710, 2015.
[36] J. Li, G. Hu, L. Shi, N. He, D. Li, Q. Shang, Q. Zhang, H. Fu, L. Zhou, W. Xiong, J. Guan, J. Wang, S. He, and L. Chen, "Full-color enhanced second harmonic generation using rainbow trapping in ultrathin hyperbolic metamaterials," *Nature Commun.*, vol. 12, no. 1, pp. 8–13, Nov. 2021.
[37] K. Liu, X. Zeng, S. Jiang, D. Ji, H. Song, N. Zhang, and Q. Gan, "A large-scale lithography-free metasurface with spectrally tunable super absorption," *Nanoscale*, vol. 6, no. 11, pp. 5599–5605, 2014.
[38] N. Mou, X. Liu, T. Wei, H. Dong, Q. He, L. Zhou, Y. Zhang, L. Zhang, and S. Sun, "Large-scale, low-cost, broadband and tunable perfect optical absorber based on phase-change material," *Nanoscale*, vol. 12, no. 9, pp. 5374–5379, 2020.
[39] J. Xie, W. Zhu, I. D. Rukhlenko, F. Xiao, C. He, J. Geng, X. Liang, R. Jin, and M. Premaratne, "Water metamaterial for ultra-broadband and wide-angle absorption," *Opt. Exp.*, vol. 26, no. 4, p. 5052, 2018.
[40] J. Barnett, U. Plachetka, C. Nowak, and H. Wackerbarth, "Highly periodic Au nano-disc arrays for plasmon-resonant SERS structures on fused silica using UV-NIL based double-layer lift-off process," *Microelectronic Eng.*, vol. 172, pp. 45–48, Mar. 2017.
[41] G. Yoon, I. Kim, S. So, J. Mun, M. Kim, and J. Rho, "Fabrication of three-dimensional suspended, interlayered and hierarchical nanostructures by accuracy-improved electron beam lithography overlay," *Sci. Rep.*, vol. 7, no. 1, p. 6668, Jul. 2017.
[42] M. Horák, K. Bukvisová, V. Svarc, J. Jaskowiec, V. Krápek, and T. Sikola, "Comparative study of plasmonic antennas fabricated by electron beam and focused ion beam lithography," *Sci. Rep.*, vol. 8, no. 1, p. 9640, Jun. 2018.
[43] Y. Nishijima, A. Balcytis, S. Naganuma, G. Seniutinas, and S. Juodkazis, "Kirchhoff's metasurfaces towards efficient photo-thermal energy conversion," *Sci. Rep.*, vol. 9, no. 1, p. 8284, Jun. 2019.
[44] Y. Liang, H. Lin, K. Koshelev, F. Zhang, Y. Yang, J. Wu, Y. Kivshar, and B. Jia, "Full-Stokes polarization perfect absorption with diatomic metasurfaces," *Nano Lett.*, vol. 21, no. 2, pp. 1090–1095, Jan. 2021.
[45] P. B. Johnson and R. W. Christy, "Optical constant of the Nobel metals," *Phys. Rev. B, Condens. Matter*, vol. 6, no. 12, pp. 4370–4379, 1972.
[46] Z. Zhou, J. Li, R. Su, B. Yao, H. Fang, K. Li, L. Zhou, J. Liu, D. Stellinga, C. P. Reardon, and T. F. Krauss, "Efficient silicon metasurfaces for visible light," *ACS Photon.*, vol. 4, no. 3, pp. 544–551, 2017.
[47] S. M. Kamali, E. Arbabi, A. Arbabi, and A. Faraon, "A review of dielectric optical metasurfaces for wavefront control," *Nanophotonics*, vol. 7, no. 6, pp. 1041–1068, 2018.

[48] A. Patoux, G. Agez, C. Girard, V. Paillard, P. R. Wiecha, A. Lecestre, F. Carcenac, G. Larrieu, and A. Arbouet, "Challenges in nanofabrication for efficient optical metasurfaces," *Sci. Rep.*, vol. 11, no. 1, pp. 1–12, Mar. 2021.
[49] R. Tomescu, C. Kusko, D. Cristea, R. Calinoiu, and C. Parvulescu, "Nano-pillars metasurface modelled for perfect absorption at specific wavelengths in infrared spectral regime," *Solid State Electron. Lett.*, vol. 2, pp. 146–150, Dec. 2020.
[50] S. Chen, Z. Chen, J. Liu, J. Cheng, Y. Zhou, L. Xiao, and K. Chen, "Ultra-narrow band mid-infrared perfect absorber based on hybrid dielectric metasurface," *Nanomaterials*, vol. 9, no. 10, p. 1350, Sep. 2019.
[51] S. Zhang, K. Zhou, Q. Cheng, L. Lu, B. Li, J. Song, and Z. Luo, "Tunable narrowband shortwave-infrared absorber made of a nanodisk-based metasurface and a phase-change material $Ge_2Sb_2Te_5$ layer," *Appl. Opt.*, vol. 59, no. 21, p. 6309, 2020.
[52] K. Mavrakakis, J. H. Booske, and N. Behdad, "Narrowband, infrared absorbing metasurface using polystyrene thin films," *J. Appl. Phys.*, vol. 127, no. 7, Feb. 2020, Art. no. 074504.
[53] J. H. U. Igang, Y. Xiao, L. M. Zhou, X. Jiang, W. Qiu, W. Fei, Y. Chen, and Q. Zhan, "Ultra-narrow-band circular dichroism by surface lattice resonances in an asymmetric dimer-on-mirror metasurface," *Opt. Exp.*, vol. 30, no. 10, pp. 16020–16030, 2022.
[54] X. Zeng, D. Rosenmann, D. A. Czaplewski, J. Gao, and X. Yang, "Mid-infrared chiral metasurface absorbers with split-ellipse structures," *Opt. Commun.*, vol. 525, Dec. 2022, Art. no. 128854.

ZAKA ULLAH received the B.S. degree in telecommunication from the University of Engineering and Technology, Peshawar, in 2016, and the M.S. degree in electrical and electronic engineering, in 2021. For his final year project, the research was on fractal antennas with the University of Engineering and Technology, Peshawar. After starting a career in the antenna research field, he started a job with Huawei Pakistan Ltd., as an RF Engineer, where his main duty was to do drive tests of BTS clusters and do RF planning. Later, he joined his alma mater and started a job as a Research Associate with the Microwave and Antenna Research Laboratory; he also co-supervised research students on antenna designing. In January 2019, he joined Universiti Teknologi Petronas as a Graduate Research Assistant. He worked on the development of grapheme-based rectennas harvesters for batteryless systems in the field of electrical and electronic engineering. In 2022, he joined Al Ain University as a Research Scientist, where his research interests included metasurfaces, plasmonics, nanophotonics, and biosensing with hybrid metasurfaces. His research interests include optical antennas and graphene, nanoantennas, terahertz antennas, the fabrication of nanoantennas through lithography process, and the synthesis of graphene through CVD.

ILLANI M. NAWI (Member, IEEE) was born in Petaling Jaya, Malaysia, in 1979. She received the B.Eng. degree (Hons.) from Universiti Teknologi Petronas, Seri Iskandar, Perak, in 2002, the joint M.Sc. degree from Universiti Teknologi Petronas and the University of Southampton, Southampton, U.K., in 2003, and the M.Sc. degree in microelectronics systems design and the Ph.D. degree in electrical and electronic engineering from the University of Southampton, in 2004 and 2018, respectively.

In 2003, she has joined the teaching team with the Electrical and Engineering Department, Universiti Teknologi Petronas, as a Tutor, where she went on to work, from 2004 to 2010. In 2010, she became a Research Officer with Tohoku University, Sendai. Returning from Sendai, she was with SEGi University, Damansara, Malaysia, before pursuing her Ph.D. degree. Upon completion, she returned to her alma mater, Universiti Teknologi Petronas, for serving the Electrical and Electronic Engineering Department as a Lecturer. Her research interests include microelectronics systems design, robotics and automation, automotive-MEMS, bio-MEMS, and reliability in IC design. Her current research interests include the safety of automotive vehicles and the reliability of chips and using electronic devices in aiding agricultural-related problems.

MUATH AL-HASAN (Senior Member, IEEE) received the B.A.Sc. degree in electrical engineering from the Jordan University of Science and Technology, Jordan, in 2005, the M.A.Sc. degree in wireless communications from Yarmouk University, Jordan, in 2008, and the Ph.D. degree in telecommunication engineering from Institut National de la Recherche Scientifique (INRS), Université du Québec, QC, Canada, in 2015. From 2013 to 2014, he was with Planets Inc., CA, USA. In May 2015, he joined Concordia University, Canada, as a Postdoctoral Fellowship. He is currently an Assistant Professor with Al Ain University, Al Ain, United Arab Emirates. His current research interests include antenna design at millimeter-wave and terahertz, channel measurements in multiple-input and multiple-output (MIMO) systems, and machine learning and artificial intelligence in antenna design.

MUHAMMAD JUNAID received the B.E. degree in electronic engineering from the Dawood University of Engineering and Technology, Karachi, Pakistan, in 2007, the M.S. degree from the Department of Electrical Engineering, University of Malaya, Kuala Lumpur, Malaysia, and the Ph.D. degree from UTP, Malaysia. He was an Assistant Professor with the Electronic Engineering Department, BUITEMS, Quetta, Pakistan. His research interests include nanophotonic, nano-optical antennas, nano-material synthesis, and nano fabrications.

ISMAIL BEN MABROUK (Senior Member, IEEE) received the B.A.Sc. and M.A.Sc. degrees in electrical engineering from the University of Lille, Lille, France, in 2006 and 2007, respectively, and the Ph.D. degree in electrical engineering from the University of Quebec, Canada, in 2012. From 2007 to 2009, he was with Huawei Technologies, Paris, France. He joined the Wireless Devices and Systems (WiDeS) Group, University of Southern California, Los Angeles, CA, USA, in 2012. He is currently an Assistant Professor with the Department of Engineering, Durham University, U.K. His research interests include antenna design at millimeter-wave and THz frequencies, propagation studies for multiple-input and multiple-output (MIMO) systems, deep learning, and wireless body area network for medical applications. He was a recipient of the Abu Dhabi Award for Research Excellence (AARE), in 2018.

ABDUL REHMAN received the Ph.D. degree in information technology from Universiti Teknologi Petronas, Malaysia. He is currently working on Internet-of-Vehicles (IoV) information security. He has conducted and published significant research work. His research interests include vehicular communication, bio-sensing, information security, context awareness, and the design of intelligent systems.